International Journal of Greenhouse Gas Control 78 (2018) 413–419

Contents lists available at ScienceDirect

International Journal of Greenhouse Gas Control

journal homepage: www.elsevier.com/locate/ijggc

Numerical study of mixed working fluid in an original oxy-fuel power plant utilizing liquefied natural gas cold energy

Yixiao Han, Lei Cai*, Yanlei Xiang, Yanwen Guan*, Wenbin Liu, Lu Yu, Ying Liang

School of Environmental Science and Engineering, Huazhong University of Science and Technology, Wuhan 430074, PR China

ARTICLE INFO

Keywords:
Oxy-fuel combustion
CO_2 capture
LNG
Working fluid
H_2O content

ABSTRACT

Oxy-fuel combustion is considered one of the most promising technologies for carbon capture and storage (CCS) in power plant. The working fluid, which is composed of CO_2 and H_2O, is obligatory to moderate the combustion temperature in oxy-fuel systems. The content of H_2O in the working fluid has a significant influence on system performance. An original oxy-fuel power plant with the utilization of liquefied natural gas (LNG) cold energy is proposed, and the H_2O content in the working fluid is adjustable in the work. The results reveal that when the H_2O mass fraction is less than 0.3, the system efficiency increases with the increase of the H_2O content in the working fluid. When the H_2O mass fraction in the working fluid rises over 0.3, the system efficiency decreases with the increase of H_2O content due to the decrease of the recycling heat carried by H_2O. The optimum heat transfer effect of the recirculating H_2O is obtained when the H_2O mass fraction is 0.3, and the optimal thermal efficiency is 58.3%. Compared to dry cycle, the thermal efficiency of the proposed system is increased by 17.3% under the optimum condition.

1. Introduction

CO_2 is one of the most important greenhouse gases (GHGs) resulting from human activity due to the extensive use of fossil fuels (IEA, 2013; Olajire, 2010). Although many environment-friendly energy sources such as biomass, wind and solar have been proposed and developed as alternative energy sources (Panwar et al., 2011; Proskurina et al., 2017; Zerrahn, 2017; Manente et al., 2016), there is still a long way to go to alleviate dependence on fossil fuels.

Carbon capture and storage (CCS) technology is considered one of the most achievable technologies to reduce CO_2 emission from power plants, and it is being developed to comply with the intensification of environmental laws and policies (Fernandes-Araújo and Medeiros, 2017; Ashworth et al., 2015). Oxy-fuel combustion is regarded as a promising technology for large-scale CCS (Ghoniem, 2011; Al-Doboon et al., 2017). Compared to the conventional air combustion, the flue gas produced in oxy-fuel combustion is ready for sequestration because of the high concentration of CO_2. However, the application of oxy-fuel combustion is constrained due to the costly energy consumption in air separation unit and CO_2 capture process (Pires et al., 2011). At the state of the art of oxy-fuel combustion, the working fluid must be recycled to the combustor (COM) to moderate the high combustion temperature. According to different compositions of the working fluid in oxy-fuel combustion, the cycle mode can be divided into dry cycle (CO_2) and wet cycle (CO_2/H_2O). Some works have indicated that the system efficiency was higher in wet than dry cycles (Shaddix and Molina, 2011; Ethan et al., 2012), and more research about wet cycle is required.

Natural gas (NG) is thought to one of the cleanest energy sources from fossil fuels, and it has a considerable share in power generation. The share of the NG power generation exceeded 33% in 2016 in USA (EIA, 2016). In China, it is expected that the NG power generation load will double by 2020. Liquefied natural gas (LNG) is a common and flexible trade mode which can be transported by ships, trucks and trains. The temperature of LNG is about 110 K in tanks at the pressure of 1 bar, which is much lower than that of the ambient temperature. LNG contains enormous cold energy. Thus LNG is selected to fuel the proposed system with the use of LNG cold energy to capture CO_2 in this paper.

There are many utilizations of LNG cold energy, such as seawater desalination (Lin et al., 2017; Messineo and Panno, 2011), cold warehouses (Li et al., 2017), ocean thermal energy conversion (OTEC) system (Arcuri et al., 2015) and Kalina cycle (Wang et al., 2013). An effective utilization method of LNG cold energy is to combine it with power plant (Baris et al., 2017). Many researchers have studied the LNG oxy-fuel power plant with the utilization of LNG cold energy, such as the air separation unit (ASU) (Mehrpooya et al., 2017a,b, 2015;

* Corresponding authors.
E-mail addresses: cailei@hust.edu.cn (L. Cai), yanwenguan@hust.edu.cn (Y. Guan).

https://doi.org/10.1016/j.ijggc.2018.09.013
Received 9 April 2018; Received in revised form 15 September 2018; Accepted 19 September 2018
Available online 01 October 2018
1750-5836/

Mehrpooya et al., 2017a), flue gas cooling system and CO_2 capture (Mehrpooya and Moftakhari-Sharifzadeh, 2017c; Wu et al., 2017; Zhang et al., 2010; Alabdulkarem et al., 2012; Mehrpooya and Zonouz, 2017d). Zhang et al. (2010) presented an oxy-fuel power plant and CO_2 was selected as the working fluid. LNG cold energy was applied to liquefy the CO_2, cool down the flue gas and cool the blade of compressor. Mehdi et al. (2016) came up with a new cogeneration system which used CO_2 as the working fluid. As well as LNG cold energy, the low temperature solar energy was utilized to improve system performance. Gómez et al. (2016) put forward a novel CO_2 capture power plant employing LNG exergy. All the recoverable LNG exergy was utilized to increase the efficiency of the closed brayton cycle. Xu and Lin (2017) proposed a LNG-fired power generation system. The results showed that more than 90% of CO_2 could be captured if the flue gas temperature was less than 140 ℃. The study of Xiang et al. (2018) indicated that the working fluid composed entirely of H_2O was not suitable to moderate the combustion temperature in their system because the latent heat of vaporization of the flue gas was difficult to release. The phase-transition temperature of flue gas, which is close to the boiling point of H_2O, do not meet the heat transfer requirements. As mentioned above, many different types of NG fueled oxy-fuel power plants have been studied and most of the working fluids in the studies mentioned are pure CO_2. The study of the influence of different H_2O content in the working fluid on NG oxy-fuel combustion has not been reported.

An original oxy-fuel power system is proposed and different proportions of H_2O and CO_2 in the working fluid is considered in this paper. LNG cold energy is utilized in cooling down the flue gas and liquefying CO_2 produced in combustion. The effect of H_2O content in the working fluid on the system performance is investigated. The study is fundamental to the implementation of NG oxy-fuel systems.

2. Description of the system

The layout of the original oxy-fuel power system with the utilization of LNG cold energy is shown in Fig. 1. The power cycle can be identified as 1- 2-3 -4-18-5-26-25-24-6- 7-8 -9-10-11-1. The recirculating H_2O (1) is pumped to 120 bar (2) (Ystad et al., 2013; Xiang et al., 2018), and the high-pressure H_2O is heated to gaseous state (3) by the flue gas out of the gas turbine (GT) (7). The high pressure H_2O (3) is expanded in the steam turbine (ST) to generate power and the pressure of H_2O after expansion is 30 bar (4) (Zhang et al., 2010; Deng et al., 2004; Wang et al., 2013). Then H_2O is mixed with the recirculating CO_2 (18) prior to being sent to COM. In the studies identified previously in this paper, the H_2O ratio of the working fluid in the wet cycle model was unchangeable because it was actualized by circulating the flue gas and the proportion of flue gas was fixed. The H_2O content of the working fluid in this paper is adjustable due to the original recycle design to study the effect of H_2O content in the working fluid on system performance. The temperature of COM is elevated to 1400 ℃ (Kim et al., 2011; Alhazmy and Najjar, 2004). The flue gas expands to ambient pressure in the GT to generate power (6–7). The exhaust heat of the flue gas (7) is recovered to preheat the recirculating H_2O in the heat exchanger (HX3) and heat the recirculating CO_2 (17) in sequence. Finally, the flue gas temperature is lowered to ambient after being cooled by LNG (21) in the heat exchanger (HX2). The flue gas (10) is mainly composed of H_2O and CO_2 and the liquid H_2O (11) can be removed via the separator (SEP). The excess H_2O (12) produced by the combustion of fuel is removed from power cycle.

The CO_2 capture and recycle process is defined as 13-14-15-16-27-28 and 13-14-15-16-17-18, respectively. CO_2 and other impurity gases (O_2, N_2 and Ar) (13) leaving SEP are compressed to the condensation pressure (7 bar), then CO_2 is chilled and liquefied by LNG in the heat exchanger (HX1). The low-boiling impurity gas (O_2, N_2 and Ar) is still in the gas phase, and is released from HX1. A portion of the liquid CO_2 (28) is pumped to 110 bar in the pump (P4) and captured (Christopher et al., 2016), while the other part (16) is pumped in the pump (P3). The recirculating CO_2 is preheated in the heat exchanger (HX4) before mixing with H_2O (4), and then the mixture of CO_2 and H_2O is delivered to the COM to moderate the combustion temperature.

O_2 (26) is compressed to 30 bar in the compressor (C1). The O_2 purity is supposed to be 95% (with 2% N_2 and 3% Ar) in molar concentration, which is considered as the equilibrium point between the cost of producing O_2 and cost of improving its purity (Kvamsdal et al., 2007). The energy consumption of O_2 production is set to 720 kJ/kg O_2 (Zhang and Lior, 2006; Liu and Guo, 2011). The specific composition of O_2 (26) and LNG (19) is shown in Table 1 (Wu et al., 2017; Liu et al., 2009). The value of excess O_2 coefficient is set to 1.02 in the work (Liu et al., 2009).

Apart from LNG required for combustion, more LNG is needed to ensure that all CO_2 produced in COM can be cooled to its liquefaction temperature (Mehrpooya et al., 2016; Zhang et al., 2010; Liu et al., 2009). The utilization process of LNG cold energy is 19-20-21-22-23-24.

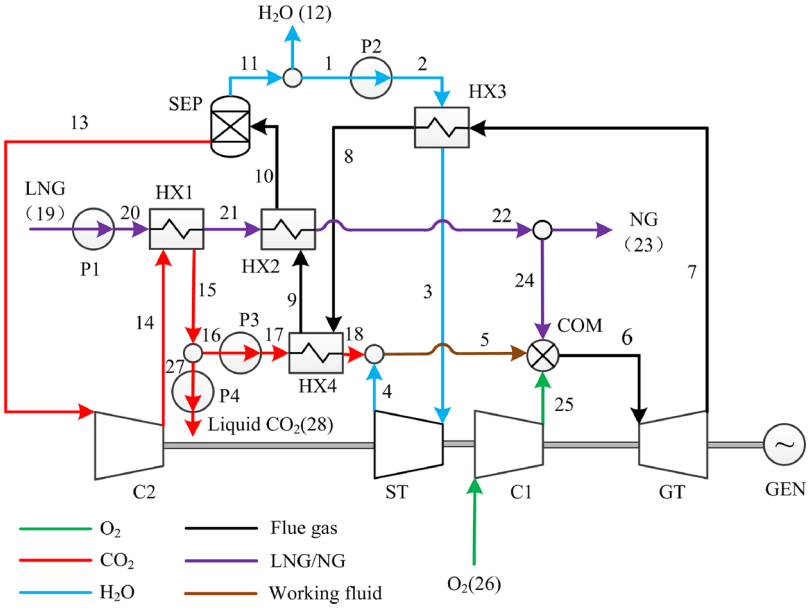

Fig. 1. The flow-process diagram of the power plant.

Table 1
Molar composition and physical properties of LNG (19) and O_2 (26).

	LNG	O_2
CH_4 (%)	90.82	/
C_2H_6 (%)	4.97	/
C_3H_8 (%)	2.93	/
C_4H_{10} (%)	1.01	/
N_2 (%)	0.27	2
O_2 (%)	/	95
Ar (%)	/	3
Temperature (°C)	−161.5	15
Pressure (bar)	1.013	25
Lower heating value (kJ/kg)	49200	/
Cost of ASU (kJ/kg)	/	720

LNG (19) is pumped to the combustion pressure (30 bar) (Zhang et al., 2010) by the pump (P1). The boiling point of N_2 is lower than that of CH_4, and N_2 in LNG vaporizes rapidly in HX1, while CH_4 is still in liquid state. Hence the concentration of N_2 in LNG (21) out of HX1 can be neglected (Querol et al., 2010). Similarly, the concentration of low-boiling impurity gas (O_2, N_2 and Ar) in CO_2 (15) also can be omitted, thus the purity of captured CO_2 is nearly 100% (Mehrpooya et al., 2016; Zhang and Lior, 2006). LNG evaporates and provides cold energy for CO_2 capture (14) and the flue gas (9) in HX1 and HX2, successively. LNG turns into NG after passing through HX1 and HX2. Some of NG is used for combustion (24), and the rest (23) is sent to other users by pipeline. The transport pressure of NG is 30 bar, which is sufficient for local distribution (Bisio and Tagliafico, 2002).

Two special cases need to be stated. Firstly, when CO_2 is the only recycled fluid, several of the components including the pump (P2), HX3 and ST will be not included in this case. H_2O from SEP is discharged out of the power cycle. In the other case, when the mass flow rate of H_2O in the working fluid (R_w) is so large that it can not be vaporized absolutely in HX3, ST will not work properly due to the existence of liquid H_2O. Therefore, ST is not considered and H_2O only need to be pumped to 30 bar instead of 120 bar in P2 in this situation. H_2O (3) from HX3 is directly mixed with the recirculating CO_2 (18).

3. Calculation assumptions

The simulation was implemented using ASPEN PLUS. The Peng-Robinson equation of state is selected as the thermodynamic property. The study of the proposed system was based on the first and second laws of thermodynamics. The system was analysed for steady state operation. The pressure dropped within the pipes and equipment is set to 2% (Alabdulkarem et al., 2012). The heat transfer between the equipment and the environment as well as the kinetic and potential energy are neglected in the simulation (Mehrpooya and Moftakhari-Sharifzadeh, 2017b).

The component models are based on the energy balance and mass balance, and the relative convergence error tolerance is set to 0.01%. Some assumptions and parameters for the process modeling are reported in Table 2 (Alabdulkarem et al., 2012; Mehrpooya and Moftakhari-Sharifzadeh, 2017b). Other energy consumptions in the system are simplified and their influence on the system are included in isentropic efficiency (Deng et al., 2004; Liu et al., 2009; Wang et al., 2013; Gómez et al., 2016; Xiang et al., 2018). To ensure the normal operation of the system under the conditions shown in Table 2, the mass flow rate of H_2O (R_w) and the mass flow rate of recirculating CO_2 (R_c) is limited within the range of 0 kg/s ~ 75.6 kg/s and 39 kg/s ~ 204.6 kg/s.

The system comprises of GT, ST, SEP, COM, Cs, Ps and HXs. The energy balance in the mentioned equipment can be calculated by the following equations.

Energy balance in all HXs:

Table 2
Main assumptions in simulation.

	Parameters	Value
Gas turbine	Turbine inlet temperature (°C)	1400
	Turbine inlet pressure (bar)	30
	Outlet pressure (bar)	1.1
Steam turbine	Turbine inlet pressure (bar)	120
	Turbine outlet pressure (bar)	30
Gas/steam turbine	Isentropic efficiency (%)	92
Reference conditions	Temperature (°C)	25
	Pressure (bar)	1.013
Combustor	Pressure loss (%)	3
	Efficiency (%)	100
	Excess O_2 percent (%)	2
Heat exchanger	Pressure loss (%)	3
	Minimum temperature difference (°C)	10
CO_2 capture	Trapping pressure (bar)	110
	Trapping temperature (°C)	−50
	Purity(%)	100
	Capture rate(%)	100
Pump	Isentropic efficiency (%)	90
Compressor	Isentropic efficiency (%)	88
Liquefied natural gas	Storage temperature (°C)	−162
	Storage pressure (bar)	1.3
Natural gas	Mass flow rate as fuel (kg/s)	8.8

$$\sum m_{in}h_{in} = \sum m_{out}h_{out} \tag{1}$$

In which m and h represent the mass flow rate and specific enthalpy, respectively.

Energy balance in all Ps and Cs:

$$W = \frac{m_{in}(h_{out} - h_{in})}{\eta_E} \tag{2}$$

In which W and η_E represents the power consumption or power output and the equipment efficiency, respectively.

Energy balance in GT and ST:

$$W = m_{in}(h_{in} - h_{out}) \times \eta_E \tag{3}$$

Heat loss from the COM is omitted due to its negligible impact on system performance (Zhang et al., 2010), the energy equation for COM is defined as:

$$m_{fuel}LHV = \frac{\sum m_{out}h_{out} - \sum m_{in}h_{in}}{\eta_E} \tag{4}$$

In which LHV represents the specific lower heating value of NG.

The thermal power generation efficiency of the system (η_{th}) can be defined as:

$$\eta_{th} = \frac{W_{net}}{m_{fuel}LHV} \tag{5}$$

In which W_{net} is defined as:

$$W_{net} = W_{GT} + W_{ST} - \sum W_C - \sum W_P - W_{ASU} \tag{6}$$

4. Results and discussion

The electric power generation capacity of the plant is affected by the composition of the working fluid, and R_w is selected as the key parameter in order to find the optimum proportion of H_2O in the working fluid. Considering that the flue gas heat-recovery process and phase transition of recirculating H_2O is actualized in HX3, the heat transfer process in HX3 is studied in detail.

4.1. Heat transfer process in HX3

Most of the regenerative heat from flue gas is transferred by recirculating H_2O through HX3, thus the heat transfer process between

Table 3
Characteristic of four conditions.

Item	ζ_w = 0.13	ζ_w = 0.3	ζ_w = 0.43	ζ_w = 0.64
H_2O temperature (3)	high	high	low	low
Q	low	high	high	high
Vapour fraction (3)	= 1	= 1	= 1	< 1
Characteristic	Half of the maximum Q	Maximum Q	Maximum ζ_w when vapour fraction (3) = 1	Maximum ζ_w

the high temperature flue gas and the low temperature recirculating H_2O is studied in this section. Four values of R_w (25 kg/s, 54 kg/s, 65 kg/s, 75 kg/s), which represent four different heat transfer conditions, are selected to analyze the heat transfer process in HX3. The mass fraction of H_2O in working fluid (ζ_w) corresponding to the four specific values of R_w is 0.13, 0.3, 0.43 and 0.64, respectively. The heat transfer capacity (Q) is chosen as the abscissa of the diagram in order to intuitively reveal the heat transfer process. The characteristic of these four conditions are shown in Table 3 to clarify the basis of the selection.

Fig. 2 shows the heat transfer process in HX3 with ζ_w = 0.13. The heat transfer process of recirculating H_2O is identified as 2–3 in Fig. 1 and Fig. 3. The recirculating H_2O (2) is heated to the boiling temperature (324 ℃) under the pressure of 120 bar prior to the evaporation process. The temperature keeps unchangeable until the recirculating H_2O is completely evaporated to steam (a-b), and the temperature of H_2O increases rapidly after the evaporation process (b-3). The heat transfer process of the flue gas is identified as 7–8 in Fig. 1 and Fig. 3. A high temperature difference between flue gas and recirculating H_2O exists throughout the heat transfer process. The temperature of flue gas after the heat transfer process is 414 ℃ (8).

Fig. 3 illustrates the heat transfer process in HX3 with ζ_w = 0.3. Since ζ_w increases from 0.13 to 0.3, the temperature difference between the flue gas and the recirculating H_2O is greatly decreased, implying that the heat exchange efficiency in HX3 reaches a high level. The value of Q in Fig. 4 reaches 190 MW after heat transfer process, which is approximately twice as much as that in Fig. 3. Due to the sufficient heat exchange process, the flue gas outlet temperature is 85 ℃.

When ζ_w increases to 0.43, the heat transfer process in HX3 is displayed in Fig. 5. The recuperative heat from flue gas only can evaporate the recirculating H_2O (2-a-3). Q in Fig. 5 is 10 MW lower than that in Fig. 4. However, the outlet temperature of H_2O (3) is 324 ℃ with ζ_w = 0.43, which is much lower than the case of ζ_w = 0.3. A large amount of heat is consumed in absorbing the latent heat of the recirculating H_2O (a–b), thus the temperature of heated H_2O (3) only reaches the saturation temperature (324 ℃). The temperature difference between the inlet flue gas (7) and the outlet H_2O (3) is 338 ℃.

Fig. 5 shows the heat transfer process with ζ_w = 0.64. The minimum

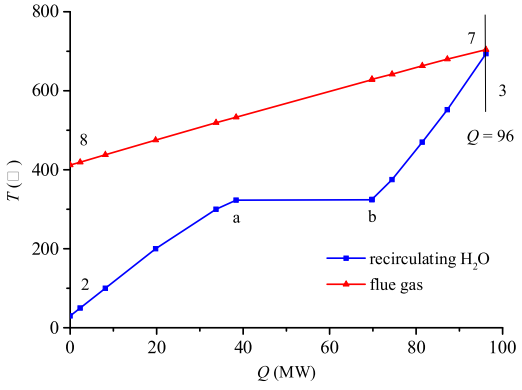

Fig. 2. Heat transfer process in HX3 with ζ_w = 0.13.

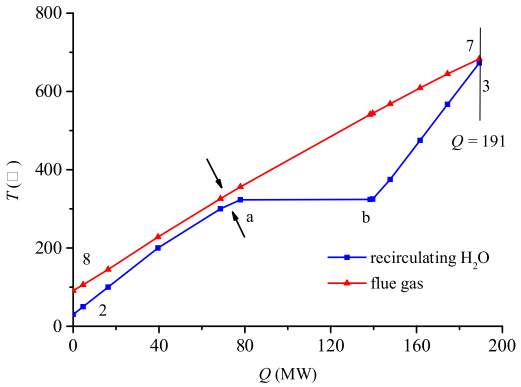

Fig. 3. Heat transfer process in HX3 with ζ_w = 0.3.

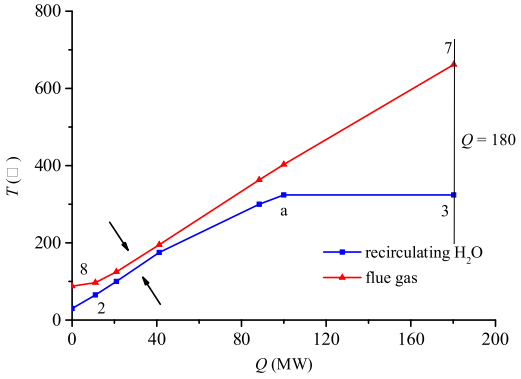

Fig. 4. Heat transfer process in HX3 with ζ_w = 0.43.

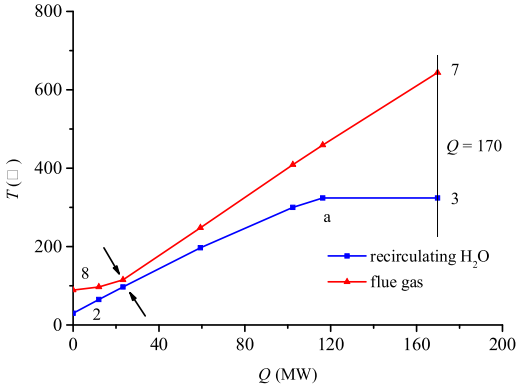

Fig. 5. Heat transfer process in HX3 with ζ_w = 0.64.

temperature difference between the hot flow and cold flow (shown by the arrow) continue to decrease when the value of ζ_w increases from 0.43 to 0.64. When ζ_w reaches 0.64, the minimum temperature difference is so small (12 ℃) that any increment of ζ_w will end the heat transfer process. 0.64 can be considered as the critical value of ζ_w. The vapour fraction of H_2O leaving HX3 is 0.59. If ζ_w keeps growing, the heat transfer will stop when the temperature of the recirculating H_2O reaches 100 ℃ due to the low heat transfer temperature difference. The vapor fraction of cold flow is 0 in this condition. If the recirculating H_2O with liquid state is sent to COM, large amount of heat will be consumed to evaporate and heat the recirculating H_2O. Although less working fluid is needed under this circumstance, the simulation results show that the thermal efficiency will be severely reduced, as displayed in the following sections.

In fact, the recirculating H_2O can not be completely evaporated when the value of ζ_w is greater than 0.43. The existence of liquid H_2O will prevent the ST from operating correctly, so ST is not considered in

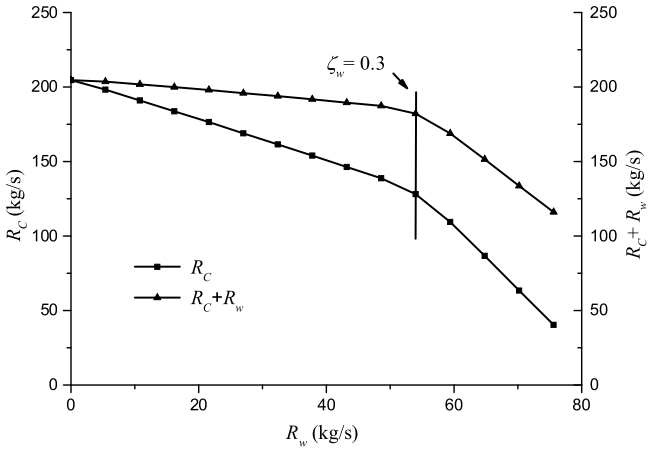

Fig. 6. R_c and R_w + R_c vary with R_w.

this case. The power generation capacity of the power plant will be weakened, which is not a rational choice.

4.2. Relationship between R_w and R_c

The GT inlet temperature and the combustion temperature in COM is assumed to be fixed at 1400 ℃. When R_w changes, R_c should be adjusted to an appropriate value to keep the temperature constant. Thus the corresponding relationship between R_w and R_c is confirmed, as shown in Fig. 6. When R_w increases, less R_c is needed to moderate the combustion temperature. Interestingly, when R_w reaches a specific point, the proportional relationship between R_w and R_c changes sharply. As shown in Fig. 6, the slope of the relationship curve changed from gentle to steep as long as R_w exceeds 54 kg/s, and the corresponding mass fraction of H_2O in the working fluid (ζ_w) is 0.3. When R_w increases from 0 to 54 kg/s, the regenerative heat carried by the recycled H_2O increases from 0 to 191 MW. Consequently, the moderating effect of the recycled H_2O is weakened, and R_c decreases slowly with the increment of R_w. When R_w increases from 54 kg/s to 75 kg/s, the regenerative heat carried by the recycled H_2O decreases from 191 MW to 170 MW and R_c decreases sharply with the increment of R_w.

4.3. Generating capacity of GT and ST

Fig. 7 shows the profile of the power generating capacity of GT and ST against R_w. For GT, when R_w < 54 kg/s (ζ_w < 0.3), more heat (147 MW) is transferred to COM when R_w increases from 0 to 54 kg/s. When R_w > 54 kg/s (ζ_w > 0.3), the power output decreases rapidly due

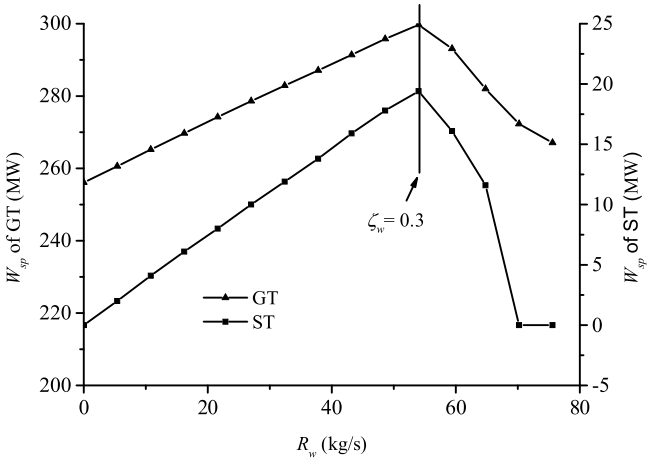

Fig. 7. Power output of GT and ST vary with R_w.

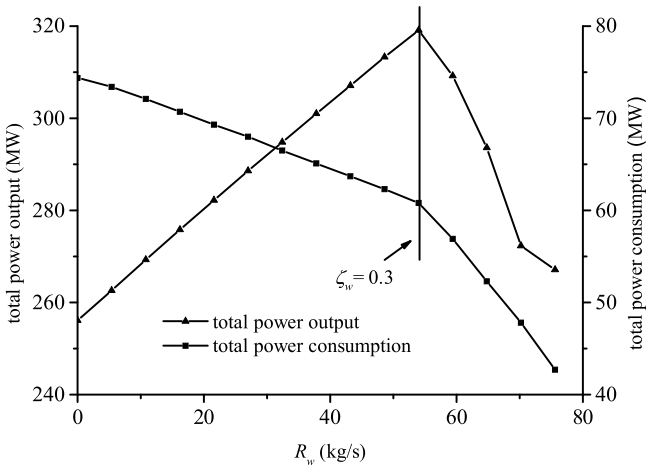

Fig. 8. Total power output and total consumption vary with R_w.

to the decrease of the temperature of heated recirculating H_2O. For ST, when R_w < 54 kg/s (ζ_w < 0.3), the outlet temperature of H_2O in HX3 stays at a high level and the power output of ST increases quickly with the increase of R_w. When R_w ranges between 54 kg/s and 65 kg/s (0.3 < ζ_w < 0.43), the power output decreases rapidly because of the decreased ST inlet temperature. The results show that the inlet temperature of ST has great effect on power output. ST is not considered in the system when 65 kg/s < R_w < 75 kg/s (0.43 < ζ_w < 0.64). The power output of ST reaches the maximum value when R_w = 54 kg/s (ζ_w = 0.3). Considering that the heat recovery efficiency in HX3 reaches the maximum value, the power output of GT also reaches the maximum value in this condition.

4.4. The total power output and consumption

Fig. 8 shows the variation of total power output and power consumption with R_w. The total power output is defined as the summation of GT and ST. When R_w < 54 kg/s (ζ_w < 0.3), the total power output increases with the increase of R_w. The total power output decreases with the increasing of R_w when R_w > 54 kg/s (ζ_w > 0.3). The total power consumption decreases with the increase of R_w, and the slope of the curve changes from gentle to steep when R_w > 54 kg/s (ζ_w > 0.3). The change of total energy expenditure will be obviously influenced by the power consumption of compressor (C2), which is directly affected by the flow rate of the recirculating CO_2.

The operation parameters of each unit or equipment under the condition of ζ_w = 0.3 are shown in Table 4. The devices that consume power include C1, C2, P1, P2, P3, P4 and ASU. The simulation results show that the power consumption of C2 and ASU always makes up a large part of the total expenditure (more than 80%). The consumption of pumps only takes a little part in total power expenditure, and the cost

Table 4
Operation parameters of equipment in power cycle.

Equipment/unit	Power consumption (MW)	Percentage (%)	Power generation (MW)	Percentage (%)
GT	–	–	298.8	93.9
ST	–	–	19.4	6.1
C1	0.83	1.2	–	–
C2	33.6	50.2	–	–
P1	4.5	6.7	–	–
P2	1.25	1.9	–	–
P3	0.62	0.9	–	–
P4	0.32	0.5	–	–
ASU	25.8	38.6	–	–

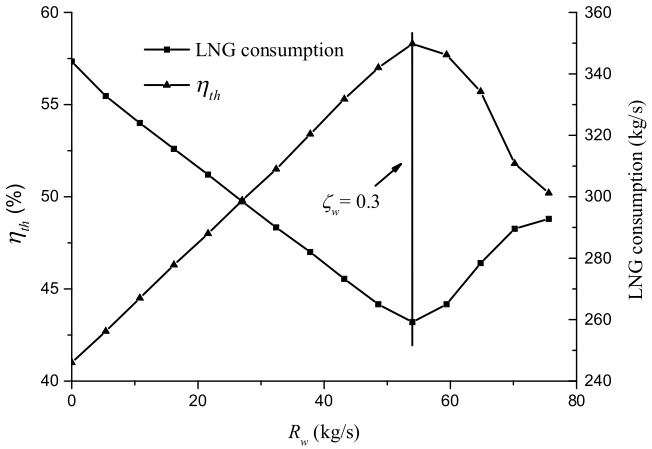

Fig. 9. η_{th} and LNG consumption vary with R_w.

of ASU unit and C1 remains unchanged as long as the specific mass flow rate of NG is kept as a fixed value. Thus the variation trend of total power consumption is in line with R_c, as shown in Fig. 6 and Fig. 8.

4.5. Thermal efficiency and LNG consumption

Fig. 9 shows the thermal efficiency and LNG consumption vary with R_w. As shown in Fig. 9, the thermal efficiency of dry cycle ($R_w = 0$) in this power plant is 41%. For $0 < R_w < 54$ kg/s ($0 < \zeta_w < 0.3$), due to the increment of regenerate heat carried by the recirculating H_2O, the thermal efficiency increases from 41.0% to 58.3% with the increase of R_w. In the region $R_w > 54$ kg/s ($\zeta_w > 0.3$), the net power output decreases sharply even though the total power consumption decreases at the same time, the decrease of regenerate heat leads to the reduction of the thermal efficiency. The thermal efficiency reaches 58.3% with $R_w = 54$ kg/s ($\zeta_w = 0.3$), which is increased by 17.3% compared to the dry cycle. The system efficiency is obviously improved when H_2O is added to the working fluid, and this result is consistent with the work done by Shaddix and Molina (2011) and Ethan et al. (2012).

The comparisons between this study and related studies (Zhang et al., 2010; Gómez et al., 2016; Deng et al., 2004) are shown in Table 5. Compared to other related systems, the system efficiency of this study is increased by 3–7.8%. To enhance the applicability of NG oxy-fuel combustion plants, further research about wet cycle is needed to be conducted in detail.

The LNG consumption profile shows an opposite tendency with η_{th}, as seen from Fig.9. For $0 < R_w < 54$ kg/s ($0 < \zeta_w < 0.3$), more heat is transferred from flue to the recirculating H_2O with the increment of R_w, thus less LNG is needed to cool down the flue gas. In the region $R_w > 54$ kg/s ($\zeta_w > 0.3$), more LNG is needed to cool down the flue gas due the decrease of heat exchange in HX3. The optimal thermal efficiency is obtained when the flow rate of LNG reaches the minimum value at 259.2 kg/s. The vaporization capacity is about 12 billion standard cubic meter of natural gas per year in this situation after calculation.

Table 5
Comparison between this study and related studies.

System	Working fluid	Fuel and combustion promoter	Thermal efficiency (%)
NGCC + CO_2 capture	CO_2+H_2O	LNG + O_2	58.3
	CO_2	LNG + O_2	41.0
COOLEP (Zhang et al., 2010)	CO_2	LNG + O_2	52.0
CBC + CO_2 capture (Gómez et al., 2016)	CO_2	LNG + O_2	55.3
COOLEP (Deng et al., 2004)	CO_2	LNG + O_2	50.5

Table 6
Thermodynamic parameters of each flow in the system.

Node	Fluid	T (℃)	p (bar)	h (kJ/kg)	s (K^{-1}·kJ/kg)
1	H_2O	30.0	1.00	22.4	0.08
2	H_2O	30.2	120.00	134.4	0.07
3	H_2O	668.9	116.41	3765.9	6.81
4	H_2O	450.9	30.00	3344.7	6.98
5	Working fluid	233.6	29.60	997.2	1.21
6	Flue gas	1400.0	28.70	2970.1	4.22
7	Flue gas	678.9	1.1	1753.5	4.20
8	Flue gas	84.9	1.07	878.6	2.18
9	Flue gas	80.6	1.04	656.9	1.41
10	Flue gas	30.0	1.00	−14.2	1.09
11	H_2O	30.0	1.00	22.4	0.08
13	CO_2	30.0	1.00	34.0	0.63
14	CO_2	232.9	7.20	224.1	0.74
15	CO_2	−50.0	7.00	−381.9	−1.54
16	CO_2	−50.0	7.00	−381.9	−1.54
17	CO_2	−48.9	30.00	−379.5	−1.53
18	CO_2	70.6	30.00	14.5	−0.05
19	LNG	−161.5	1.01	−5.3	0.01
20	LNG	−161.0	30.00	22.4	0.01
21	LNG	−96.2	29.10	237.5	2.40
22	NG	30.0	28.22	954.6	4.89
23	NG	30.0	28.22	954.6	4.89
24	NG	30.0	28.22	954.6	4.89
25	O_2	15.0	25.00	−15.0	−0.84
26	O_2	36.3	30.00	29.6	−0.83
27	CO_2	−50.0	7.00	−381.9	−1.54
28	CO_2	−43.7	110.00	−367.1	−1.52

The thermodynamic parameters under the condition of $\zeta_w = 0.3$ for each point of the system are summarized in Table 6, and the mass flow rate and molar composition of each node in the system are shown in Table 7.

5. Concluding remarks

An original CO_2-capturing oxy-fuel power system using the cold

Table 7
Mass flow rate and molar compositions of the system.

Node	m (kg/s)	O_2 (%)	CO_2 (%)	H_2O (%)	N_2 (%)	Ar (%)	LNG/NG (%)
1	54.0	/	/	100	/	/	/
2	54.0	/	/	100	/	/	/
3	54.0	/	/	100	/	/	/
4	54.0	/	/	100	/	/	/
5	182.4	/	49.43	50.57	/	/	/
6	227.1	0.29	45.44	53.51	0.30	0.46	/
7	227.1	0.29	45.44	53.51	0.30	0.46	/
8	227.1	0.29	45.44	53.51	0.30	0.46	/
9	227.1	0.29	45.44	53.51	0.30	0.46	/
10	227.1	0.29	45.44	53.51	0.30	0.46	/
11	101.6	/	/	100	/	/	/
13	153.2	0.62	97.74	/	0.65	0.99	/
14	153.2	0.62	97.74	/	0.65	0.99	/
15	153.2	/	100	/	/	/	/
16	129.0	/	100	/	/	/	/
17	129.0	/	100	/	/	/	/
18	129.0	/	100	/	/	/	/
19	259.2	/	/	/	/	/	1
20	259.2	/	/	/	/	/	1
21	259.2	/	/	/	/	/	1
22	259.2	/	/	/	/	/	1
23	250.4	/	/	/	/	/	1
24	8.8	/	/	/	/	/	1
25	35.9	95	/	/	2	3	/
26	35.9	95	/	/	2	3	/
27	24.2	/	1	/	/	/	/
28	24.2	/	1	/	/	/	/

energy of liquefied natural gas (LNG) is proposed in this paper. The effect of different H_2O ratios in the working fluid on the system performance and the heat transfer process in the heat exchanger (HX3) is studied. The exergy analysis and techno-economic assessment are also important for the implementation of the system, and it will be conducted in our future work. The main conclusions are stated as follows:

1 When the mass fraction of H_2O in working fluid (ζ_w) is lower than 0.3, the heat from the flue gas is sufficient to heat the recirculating H_2O. The regenerative heat increases rapidly with the increase of ζ_w, thus the system performance is greatly improved.
2 When $0.3 < \zeta_w < 0.64$, the temperature difference between outlet H_2O of HX3 and the flue gas is higher than 300 ℃. Although less the working fluid is needed, a large amount of heat is consumed to heat the recirculating H_2O. The system efficiency decreases with the increase of ζ_w.
3 When $\zeta_w > 0.64$, the heat transfer will stop when the temperature of the recirculating H_2O reaches 100 ℃ due to the low heat transfer temperature difference.
4 The simulation results show that when $\zeta_w = 0.3$, the optimal thermal efficiency is raised to 58.3%. Compared to the dry cycle, the thermal efficiency is increased by 17.3% under the optimum condition. Compared to other related systems (Zhang et al., 2010; Gómez et al., 2016; Deng et al., 2004), the system efficiency of this study is increased by 3–7.8%.

Acknowledgment

This work was supported by the Fundamental Research Funds for the Central Universities (2017KFYXJJ214).

References

Alabdulkarem, A., Hwang, Y., Radermacher, R., 2012. Energy consumption reduction in CO_2 capturing and sequestration of an LNG plant through process integration and waste heat utilization. Int. J. Greenhouse Gas Control 10, 215–228.
Al-Doboon, A., Gutesa, M., Valera-Medina, A., Syred, N., Ng, J.H., Chong, C.T., 2017. CO_2-argon-steam oxy-fuel (CARSOXY) combustion for CCS inert gas atmospheres in gas turbines. Appl. Therm. Eng. 122, 350–358.
Alhazmy, M.M., Najjar, Y.S.H., 2004. Augmentation of gas turbine performance using air coolers. Appl. Therm. Eng. 24, 415–429.
Arcuri, N., Bruno, R., Bevilacqua, P., 2015. LNG as cold heat source in OTEC systems. Ocean. Eng. 104, 349–358.
Ashworth, P., Wade, S., Reiner, S., Liang, X., 2015. Developments in public communications on CCS. Int. J. Greenhouse Gas Control 40, 449–458.
Baris, B.K., Xiang, L.M., Swapnil, D., Fook, H.C., Duan, F., 2017. Cold utilization systems of LNG: a review. Renewable Sustainable Energy Rev. 79, 1171–1188.
Bisio, G., Tagliafico, L., 2002. On the recovery of LNG physical exergy by means of a simple cycle or a complex system. Int. J. Exergy 2 (1), 34–50.
Christopher, J.W., Michael, F., Samuel, A.E.G., Robert, M.W., Abigail, M.E.W., 2016. High pressure CO_2 CCS pipelines: comparing dispersion models with multiple experimental datasets. Int. J. greenhouse gas control 54, 716–726.
Deng, S.M., Jin, H.G., Cai, R.X., Lin, R.M., 2004. Novel cogeneration power system with liquefied natural gas (LNG) cryogenic exergy utilization. Energy 29, 497–512.
Energy Information Administration, 2016. Annual Energy Outlook. EIA publishing Inc., Washington.
Ethan, S.H., Christopher, R.S., Manfred, G., Alejandro, M., Brian, S.H., 2012. Effect of CO_2 and steam gasification reactions on the oxy-combustion of pulverized coal char. Combust. Flame 159, 3437–3447.
Fernandes-Araújo, O.Q., Medeiros, J.L., 2017. Carbon capture and storage technologies: present scenario and drivers of innovation. Curr. Opin. Chem. Eng. 17, 22–34.
Ghoniem, A.F., 2011. Needs, resources and climate change: clean and efficient conversion technologies. Prog. Energy Combust. Sci. 37, 15–51.
Gómez, M.R., Gómez, J.R., López-González, L.M., López-Ochoa, L.M., 2016. Thermodynamic analysis of a novel power plant with LNG (liquefied natural gas) cold exergy exploitation and CO_2 capture. Energy 105, 32–44.
International Energy Agency, 2013. World Energy Outlook. IEA publishing Inc., Paris.
Kim, Y.S., Lee, J.J., Kim, T.S., Sohn, J.L., 2011. Effects of syngas type on the operation and performance of a gas turbine in integrated gasification combined cycle. Energy Convers. Manage. 52, 2262–2271.
Kvamsdal, H.M., Jordal, K., Bolland, O., 2007. A quantitative comparison of gas turbine cycles with CO_2 capture. Energy. Energy 32, 10–24.
Li, S., Wang, B., Dong, J.K., Jiang, Y.Q., 2017. Thermodynamic analysis on the process of regasification of LNG and its application in the cold warehouse. Therm. Sci. Eng. Prog. 4, 1–10.
Lin, W.S., Huang, M.B., Gu, A.Z., 2017. A seawater freeze desalination prototype system utilizing LNG cold energy. Int. J. Hydrogen Energy 42, 18691–18698.
Liu, Y., Guo, K., 2011. A novel cryogenic power cycle for LNG cold energy recovery. Energy 36, 2828–2833.
Liu, M., Lior, M., Zhang, N., Han, W., 2009. Thermoeconomic analysis of a novel zero-CO_2-emission high-efficiency power cycle using LNG coldness. Energy Convers. Manage. 50, 2768–2781.
Manente, G., Rech, S., Lazzaretto, A., 2016. Optimum choice and placement of concentrating solar power technologies in integrated solar combined cycle systems. Renew. Energy 96, 172–189.
Mehrpooya, M., Moftakhari-Sharifzadeh, M.M., 2017b. Conceptual and basic design of a novel integrated cogeneration power plant energy system. Energy 127, 516–533.
Mehrpooya, M., Moftakhari-Sharifzadeh, M.M., 2017c. A novel integration of oxy-fuel cycle, high temperature solar cycle and LNG cold recovery–energy and exergy analysis. Appl. Therm. Eng. 114, 1090–1104.
Mehrpooya, M., Mehdi, M., Sharifzadeh, M., Rosenc, M.A., 2015. Optimum design and exergy analysis of a novel cryogenic air separation process with LNG (liquefied natural gas) cold energy utilization. Energy 90, 2047–2069.
Mehrpooya, M., Moftakhari, S.M.M., Rosen, M.A., 2016. Energy and exergy analyses of a novel power cycle using the cold of LNG (liquefied natural gas) and low-temperature solar energy. Energy 95, 324–345.
Mehrpooya, M., Esfilarc, R., Ali-Moosavianc, S.M., 2017a. Introducing a novel air separation process based on cold energy recovery of LNG integrated with coal gasification, transcritical carbon dioxide power cycle and cryogenic CO_2 capture. J. Cleaner Production 142, 1749–1764.
Mehrpooya, M., Zonouz, M.J., 2017d. Analysis of an integrated cryogenic air separation unit, oxy-combustion carbon dioxide power cycle and liquefied natural gas regasification process by exergoeconomic method. Energy Convers. Manage. 139, 245–259.
Messineo, A., Panno, G., 2011. LNG cold energy use in agro-food industry: a case study in Sicily. J. Natural Gas Science and Engineering 3, 356–363.
Olajire, A.A., 2010. CO_2 capture and separation technologies for end-of-pipe applications - a review. Energy 35, 2610–2628.
Panwar, N.L., Kaushik, S.C., Kothari, S., 2011. Role of renewable energy sources in environmental protection: a review. Renew. Sustain. Energy Rev. 15, 1513–1524.
Pires, J.C.M., Martins, F.G., Alvim-Ferraz, M.C.M., Simões, M., 2011. Recent developments on carbon capture and storage:an overview. Chem. Eng. Res. Des. 89, 1446–1460.
Proskurina, S., Heinimö, J., Schipfer, F., Vakkilainen, E., 2017. Biomass for industrial applications: the role of torrefaction. Renew. Energy 111, 265–274.
Querol, E., Gonzalez-Regueral, B., García-Torrent, J., García-Martínez, M.J., 2010. Boil off gas (BOG) management in Spanish liquid natural gas (LNG) terminals. Appl. Energy 87, 3384–3392.
Shaddix, C., Molina, A., 2011. Ignition, flame stability, and char combustion in oxy-fuel combustion. In: Zheng, L.G. (Ed.), Oxy-Fuel Combustion for Power Generation and Carbon Dioxide (CO_2) Capture. Woodhead Publishing Inc., Cambridge, pp. 101–124.
Wang, H., Shi, X.J., Che, D.F., 2013. Thermodynamic optimization of the operating parameters for a combined power cycle utilizing low-temperature waste heat and LNG cold energy. Appl. Therm. Eng. 59, 490–497.
Wu, J.F., Chen, Y.P., Zhu, Z.L., Mei, X.Z., Zhang, S.B., Zhang, B.H., 2017. Performance simulation on NG/O_2 combustion gas and steam mixture cycle with energy storage and CO_2 capture. Appl. Energy 196, 68–81.
Xiang, Y.L., Cai, L., Guan, Y.W., Liu, W.B., Han, Y.X., Liang, Y., 2018. Study on the configuration of bottom cycle in natural gas combined cycle power plants integrated with oxy-fuel combustion. Appl. Energy 212, 465–477.
Xu, J.X., Lin, W.S., 2017. A CO_2 cryogenic capture system for flue gas of an LNG-fired power plant. Int. J. Hydrogen Energy 42, 18674–18680.
Ystad, P.A.M., Lakew, A.A., Bolland, O., 2013. Integration of low-temperature transcritical CO_2 Rankine cycle in natural gas-fired combined cycle (NGCC) with post-combustion CO_2 capture. Int. J. Greenhouse Gas Control 12, 213–219.
Zerrahn, A., 2017. Wind power and externalities. Ecol. Econ. 141, 245–260.
Zhang, N., Lior, N., 2006. A novel near-zero CO_2 emission thermal cycle with LNG cryogenic exergy utilization. Energy 31, 1666–1679.
Zhang, N., Lior, N., Liu, M., Han, W., 2010. COOLCEP (cool clean efficient power): a novel CO_2-capturing oxy-fuel power system with LNG (liquefied natural gas) coldness energy utilization. Energy 35, 1200–1210.